

Original Research

ARHGAP6 Suppresses Breast Cancer Tumor Growth by Promoting Ferroptosis via RhoA-ROCK1-p38 MAPK Signaling

Xiaoqing Chen^{1,†}, Jing Zhu^{1,†}, Xiangzhi Li¹, Jintao Chen¹, Zhisheng Zhou¹, Xulong Fan¹, Ruijian Liang¹, Haiyan Liu¹, Dajiang Zhu^{1,*}¹Department of Breast Medicine, Southern Medical University Affiliated Maternal & Child Health Hospital of Foshan, 528000 Foshan, Guangdong, China*Correspondence: zhudajiang@163.com (Dajiang Zhu)

†These authors contributed equally.

Academic Editor: Amedeo Amedei

Submitted: 10 July 2023 Revised: 21 August 2023 Accepted: 24 August 2023 Published: 12 January 2024

Abstract

Background: Ferroptosis, a distinct iron-dependent form of regulated cell death, is induced by severe lipid peroxidation due to reactive oxygen species (ROS) generation. Breast cancer patient survival is correlated with the tumor-suppressing properties of Rho guanosine triphosphatase hydrolase enzyme (GTPase)-activating protein 6 (ARHGAP6). This study investigates the impact and mechanisms of ARHGAP6 on ferroptosis in breast cancer. **Methods:** Using quantitative RT-PCR, Western blotting, and immunofluorescence staining, ARHGAP6 expression was detected in a gene expression dataset, cancer tissue samples, and cells. ARHGAP6 was overexpressed or silenced in breast cancer cell lines. Cell proliferation was measured using 5-ethynyl-2-deoxyuridine (EdU) assay, and cell death rate was determined using LDH cytotoxicity assay. As indicators of ferroptosis, Fe²⁺ ion content, lipid ROS, glutathione peroxidase 4 (GPX4), ChaC glutathione specific gamma-glutamylcyclotransferase 1 (CHAC1), prostaglandin-endoperoxide synthase 2 (PTGS2), solute carrier family 7 member 11 (SLC7A11), and acyl-CoA synthetase long chain family member 4 (ACSL4) levels were evaluated. **Results:** ARHGAP6 was obviously downregulated in cancer tissues and cells. ARHGAP6 overexpression decreased cell proliferation, elevated cell death and lipid ROS, decreased GPX4 and SLC7A11, increased PTGS2, ACSL4, and CHAC1, and inhibited RhoA/ROCK1 and p38 MAPK signaling in cancer cells. ARHGAP6 knockdown exerted opposite effects to those of ARHGAP6 overexpression. p38 signaling suppression reversed the effect of ARHGAP6 knockdown on ferroptosis, while RhoA/ROCK1 signaling inhibition compromised the effect of ARHGAP6 on p38 MAPK signaling. In mice models, ARHGAP6 together with the ferroptosis inducer RSL3 cooperatively enhanced ferroptosis and inhibited tumor growth of cancer cells. ARHGAP6 mRNA level was positively correlated with that of ferroptosis indicators in tumor tissues. **Conclusions:** This study revealed that ARHGAP6 inhibited tumor growth of breast cancer by inducing ferroptosis via RhoA/ROCK1/p38 MAPK signaling. Integrating ARHGAP6 with ferroptosis-inducing agents may be a promising therapeutic strategy for breast cancer treatment.

Keywords: breast cancer; ARHGAP6; ferroptosis; p38 MAPK

1. Introduction

Breast cancer leads to the fifth mortality rate among all female cancer diseases and has a 6.6% mortality rate [1,2]. In recent years, breast cancer treatment includes refined surgical resection, chemotherapy, radiotherapy, targeted therapy, and endocrine therapy [3]. However, breast cancer patients' survival remains unfavorable [4]. Therefore, extensive efforts are urgently needed to design and develop novel effective therapeutic strategies for breast cancer patients.

Ferroptosis is an iron-dependent type of nonapoptotic cell death accompanied by mitochondrial alterations due to increased reactive oxygen species (ROS) accumulation resulting from excessive lipid peroxidation [5]. Glutathione peroxidase 4 (GPX4) converts reduced GSH to oxidized GSSG and reduces excess oxidized lipids due to the presence of ROS in the reaction [6]. Solute carrier family 7 member 11 (SLC7A11) as an anti-ferroptotic marker produces glutathione to regulate GPX4

activity [7]. Acyl-CoA synthetase long chain family member 4 (ACSL4), a positive regulator of ferroptosis, activates long-chain fatty acids for lipid synthesis, increasing cellular ferroptotic susceptibility [6]. Prostaglandin-endoperoxide synthase 2 (PTGS2) and ChaC glutathione specific gamma-glutamylcyclotransferase 1 (CHAC1) are two well-documented biomarkers of ferroptosis [8]. Ferroptosis is closely related to cancer initiation and development and contributes to the therapeutic treatment responses of various cancers including breast cancer [9]. A promising therapeutic approach to breast cancer treatment is the induction of ferroptosis to eliminate cancer cells [10,11].

Rho guanosine triphosphatase hydrolase enzyme (GTPases)-mediated signaling transduction is crucial for the progression of human malignancies [12]. Rho GTPase-activating protein 6 (ARHGAP6) regulates actin polymerization, contributing to tumor growth and metastasis [13]. Previous studies revealed that ARHGAP6 downregulation



may suppress tumor formation in bladder, breast, cervical, and lung cancer [14–17], and evidence showed that ARHGAP6 expression is related to breast cancer patients' survival [14]. Ras homolog family member A (RhoA) is a small GTPase protein that switches from GTP-bound state to GDP-bound state by hydrolyzing GTP [17]. Another study demonstrated an interaction between RhoA and p38 MAPK, which is activated in breast cancer [18]. RhoA and p38 MAPK are also associated with ferroptosis [19–21]. Nevertheless, the association of ARHGAP6 with ferroptosis and related regulatory mechanisms in breast cancer remains elusive.

This study detected ARHGAP6 expression in breast cancer tissue samples harvested from hospitalized patients, and breast cancer cell lines to elucidate the biological role of ARHGAP6. The impact of ARHGAP6 overexpression or knockdown on ferroptosis was investigated by measuring the Fe²⁺ ion content and lipid ROS levels and by detecting the protein levels of ferroptosis-related factors. Moreover, *in vitro* results were validated using *in vivo* experiments, and possible downstream signaling pathways were investigated. This study provides insights beneficial for planning future therapeutic strategies for breast cancer.

2. Materials and Methods

2.1 Bioinformatics Analysis

Gene expression data was obtained from The Cancer Genome Atlas (TCGA) database (<https://www.cancer.gov/about-nci/organization/ccg/research/structural-genomics/tcga>) that included 1104 tumor tissues and 113 normal breast tissues. Using the gene set enrichment analysis (GSEA) algorithm, pathways enriched between samples with low or high expression of ARHGAP6 were identified.

2.2 Clinical Tumor Samples

A total of 30 tumor and matched adjacent-normal tissue samples were collected from breast cancer patients at the Southern Medical University Affiliated Maternal & Child Health Hospital of Foshan. A signed informed consent was obtained from all patients. The medical ethics committee of Southern Medical University Affiliated Maternal & Child Health Hospital of Foshan (No. FSFY-MEC-2021-042) approved the present retrieval method of cancer tissue samples. To measure ARHGAP6 levels, a human breast cancer tissue microarray (Outdo Biotech Co., Ltd., Shanghai, China) containing 75 tumor tissues and 20 adjacent normal breast tissues were used.

2.3 Immunohistochemistry

Human breast cancer tissue microarray was analyzed using immunohistochemistry. Tissue slides were incubated with using anti-ARHGAP6 antibody (NBP2-49417, Novus Biologicals, LLC, Centennial, CO, USA). Using the H-score system, immunoreactivity was scored based on posi-

tively stained cells and staining intensity [22]. Breast cancer patients were classified into high-expression (H-score ≥ 4) and low-expression (H-score < 4) groups.

2.4 Cell Culture and Transfection

Human breast cancer cell lines (BT-474, MCF-7, SKBR3, and ZR751) and a nontumorigenic human breast epithelial cell line (MCF-10A) were obtained from the American Type Culture Collection (ATCC, Manassas, VA, USA) and were maintained in RPMI 1640 (11875119, Thermo Fisher Scientific, Waltham, MA, USA) media supplemented with 10% fetal bovine serum and 1% penicillin/streptomycin (Life Technologies) in a humidified incubator with an atmosphere of 5% CO₂/95% air at 37 °C. MCF-7 and ZR751 cells within the Luminal A subtype were estrogen receptor (ER) and progesterone receptor (PR) positive. BT-474 within the Luminal B subtype were ER negative, PR positive and human epidermal growth factor receptor type 2 (HER2) positive. SKBR3 cells within the HER2 overexpression subtype were ER and PR negative. All the cell lines were authenticated by short tandem repeat and were confirmed negative for mycoplasma contamination (Mycoalert Mycoplasma Detection Kit, Lonza, Switzerland).

RNA interference sequences targeting ARHGAP6 (siRNA#1 AGCAGAAGUCAUCAGACAAAG; siRNA#2 CAAUCAGUCUCGACUACUAGA; siRNA#3 CACC-GAUCUUGAUGACAAUCA) and scramble siRNA sequence (GCCUGACCAUACACUCGCUCA) were synthesized and transfected into breast cells using Lipofectamine 2000 system according to the manufacturer's protocol (11668500, Thermo Fisher Scientific, Waltham, MA, USA). Human ARHGAP6 coding cDNA sequence was synthesized by Sangon Biotech as well and inserted into the pLVX-Puro vector (QYV0008, Beijing qualityard biotechnology Co., Ltd., China). Transfection was performed using the Lipofectamine 2000 system. Subsequently, 48 h after transfection, recombinant vector in the cell supernatant was collected and transduced into breast cancer cells.

2.5 Ethynyl-2-deoxyuridine (EdU) Assay

MCF-7 cells transduced with indicated vectors were treated with or without 25 μ M apoptosis inhibitor zVAD-fmk, 20 μ M necroptosis inhibitor necrostatin-1, 10 μ M ferroptosis inhibitor ferrostatin-1, or 1 μ g/mL RSL3 (all from Selleck, Shanghai, China). BT-474 cells transfected with siARHGAP6 or siNC were treated with or without SB203580 (10 μ M; Selleck). The cells were stained according to the instructions of the BeyoClick™ EdU Cell Proliferation Kit (C0071S, Beyotime Biotechnology, Shanghai, China). Cells were then incubated with DAPI solution and were observed using fluorescence microscopy.

2.6 LDH Release Cell Death Assay

MCF-7 cells transduced with indicated vectors were treated with or without 1 $\mu\text{g}/\text{mL}$ RSL3. BT-474 cells transfected with siARHGAP6 or siNC were treated with or without 10 μM SB203580. Cell death rate was determined using the lactate dehydrogenase (LDH) cytotoxicity assay kit (Beyotime Biotechnology, Shanghai, China) as per manufacturer's instructions and calculated as previously described [23].

2.7 Lipid ROS and Iron Content Measurements

MCF-7 cells transduced with indicated vectors were treated with or without 1 $\mu\text{g}/\text{mL}$ RSL3. BT-474 cells transfected with siARHGAP6 or siNC were treated with or without 10 μM SB203580. The level of lipid ROS was quantified using C11-BODIPY (581/591) assay (D3861, Thermo Fisher Scientific, Waltham, MA, USA). Briefly, the cell suspension was added with 10 μM C11-BODIPY (581/591) and incubated for 30 min at 37 °C in the dark. Fluorescence intensity was measured using an Accuri™ C6 flow cytometer (BD Biosciences, San Jose, CA, USA). To detect for Fe^{2+} ion content, the Iron Assay Kit (ab83366, Abcam, Waltham, MA, USA) was used as per manufacturer's instructions.

2.8 Quantitative RT-PCR

Total RNA was extracted using TRIzol solution (Thermo Fisher Scientific). The first-strand cDNA was synthesized using the Hifair® II 1st Strand cDNA Synthesis SuperMix for qPCR (Yeasen Biotechnology (Shanghai) Co., Ltd., Shanghai, China) as per manufacturer's instructions. Using the Hieff® qPCR SYBR Green Master Mix (Yeasen Biotechnology (Shanghai) Co., Ltd) on an ABI 7300 real-time PCR system (Applied Biosystems, Foster, CA, USA), quantitative RT-PCR was performed. The primers used included the following: ARHGAP6-F: 5'-TG AGGTCAGTCCCCATCC-3'; ARHGAP6-R: 5'-GCATC TTTCTGCTCGTCC-3'; GPX4-F: 5'-CTCCCAGTGAGG CAAGAC-3'; GPX4-R: 5'-GTTACTCCCTGGCTCCTG-3'; PTGS2-F: 5'-TTACAATGCTGACTATGGCTAC-3'; PTGS2-R: 5'-CTGATGCGTGAAGTGCTG-3'; CHAC1-F: 5'-ACGACGGCGACCCTCAAG-3'; CHAC1-R: 5'-GGG TTCTGCTCCCCTTGC-3'; ACSL4-F: 5'-AAAAAGGTC AAGGCCCTGCT-3'; ACSL4-R: 5'-CTGTCCCAGCACC ACATGAT-3'; SLC7A11-F: 5'-CTAACTAACTGGTCC TCAACTC-3'; SLC7A11-R: 5'-CCTAAGAAACAACGC AATCC-3'; GAPDH-F: 5'-AATCCCATCACCATCTTC -3'; GAPDH-R: 5'-AGGCTGTTGTCATACTTC-3'. The relative expression level of target genes was normalized to that of GAPDH using the $2^{-\Delta\Delta\text{Ct}}$ method.

2.9 Antibodies and Western Blots

Proteins were lysed from tumor tissues and cell lines using radioimmunoprecipitation assay buffer (50 mM Tris, pH 7.4, 150 mM NaCl, 1% NP-40, 100 mM NaF) with

protease and phosphatase inhibitor cocktail. Proteins were separated by sodium dodecyl sulphate-polyacrylamide gel electrophoresis and transferred onto nitrocellulose membranes (Millipore, Billerica, MA, USA). Then, the membranes were incubated with primary antibodies against ARHGAP6 (Invitrogen; PA5-104106), ROCK1 (ab97592, Abcam, Waltham, MA, USA), GPX4 (ab125066, Abcam), PTGS2 (ab179800, Abcam), CHAC1 (ab217808, Abcam), ACSL4 (ab155282, Abcam), SLC7A11 (ab175186, Abcam), GAPDH (5174, Cell Signaling Technology, Danvers, MA, USA), p-p38 (4511, Cell Signaling Technology), and p38 (9212, Cell Signaling Technology), followed by incubation with HRP-conjugated secondary antibodies (A0208, Beyotime Biotechnology).

2.10 Measurement of RhoA Activity

MCF-7 cells were transduced with indicated vectors, and BT-474 cells transfected with siARHGAP6 or siNC were treated with or without Y-27632 (10 μM ; Selleck), and the RhoA activity was measured using a Rho Activation Assay Biochem Kit (Cytoskeleton, Denver, CO, USA).

2.11 Xenograft Experiment

MCF-7 cells (5×10^6) transduced with indicated vectors were subcutaneously injected into the flank regions of mice (4 to 5 weeks old; Shanghai Laboratory Animal Company, Shanghai, China). RSL3 (100 mg/kg) was injected twice a week. Tumor volume was recorded every three days. Thirty-three days after RSL3 injection, the mice were sacrificed, and tumors were collected ($n = 6$ per group). All animal experiments were performed according to the animal ethics guidelines of the Animal Care and Use Committee of Shanghai Rat@Mouse Biotech Co., Ltd., China [No. 202103(11)].

2.12 Immunofluorescence Microscopy

Tissues samples collected from the xenograft tumor were incubated using anti-Ki67 (ab245113, Abcam) and Alexa Fluor 488-labeled Goat anti-mouse IgG (H + L) (A0428, Beyotime Biotechnology) antibodies, followed by DAPI (C1002, Beyotime Biotechnology) labeling. Using a confocal laser scanning microscope (Leica Microsystems, Inc., Deerfield, IL, USA), the positively stained cells were then visualized.

2.13 Statistical Analysis

Statistical analysis was performed using GraphPad Prism 8.4.2 (GraphPad Software, San Diego, CA, USA). All experiments were performed in triplicate, and quantitative data were expressed as mean \pm standard deviation. The overall survival was determined using the Kaplan–Meier survival analysis and log-rank test. Comparisons between the different groups were compared using the analysis of variance test or Student's *t* test. *p* value < 0.05 was considered statistically significant.

3. Results

3.1 ARHGAP6 Downregulation was Observed in Breast Cancer Tissue and Cells

TCGA dataset gene expression data screening showed that ARHGAP6 mRNA level was decreased in tumor samples compared with normal samples (Fig. 1A). Moreover, 30 clinical tumor samples were collected from hospitalized breast cancer patients. Quantitative RT-PCR showed that the mRNA level of ARHGAP6 was markedly decreased in tumor samples compared with adjacent-normal tissues (Fig. 1B). Immunohistological staining also demonstrated a low ARHGAP6 protein expression levels in tumor samples compared with adjacent-normal tissues from human breast cancer tissue arrays (Fig. 1C). The patients with high ARHGAP6 expression (H-score ≥ 4 ; $n = 34$) had significantly improved survival time compared with those patients with low ARHGAP6 expression (H-score < 4 ; $n = 41$; Fig. 1D). ARHGAP6 expression was markedly reduced in human breast cancer cell lines (BT-474, MCF-7, SKBR3, and ZR751) compared with the nontumorigenic human breast epithelial cell line (MCF-10A), with the highest and lowest expression detected in BT-474 and MCF-7 cells, respectively (Fig. 1E,F). These two cell lines were therefore used for subsequent experiments.

3.2 ARHGAP6 Overexpression Promoted Ferroptosis and Suppressed RhoA/ROCK1 and p38 MAPK Signaling Pathways in MCF-7 Cells

To examine the role of ARHGAP6 in breast cancer, MCF-7 cells with the lowest ARHGAP6 expression compared with other breast cancer cell lines were transduced with ARHGAP6 expression vector to overexpress ARHGAP6. Following the successful establishment of ARHGAP6 overexpression, ARHGAP6 mRNA and protein levels were significantly increased (**Supplementary Fig. 1A–C**). At 48 h post-transduction, cell proliferation was decreased, and cell death was increased in ARHGAP6-overexpressing MCF-7 cells (Fig. 2A–C). To determine the cause of ARHGAP6 overexpression-induced cell death, several cell death inhibitors were tested. Ferroptosis inhibitor ferrostatin-1 markedly inhibited ARHGAP6 overexpression-induced cell death; however, apoptosis inhibitor zVAD-fmk only mildly inhibited ARHGAP6 overexpression-induced cell death (Fig. 2A–C). To further examine the effects of ferroptosis on ARHGAP6 overexpression-mediated cell death, Fe^{2+} ion content and lipid ROS levels were measured. Fe^{2+} ion content (Fig. 2D) and lipid ROS levels (Fig. 2E) were dramatically increased in ARHGAP6-overexpressing MCF-7 cells.

RhoA activates downstream Rho-related protein kinase 1 (ROCK1) and modulates the accumulation of ROS [24,25]. To detect whether RhoA/ROCK1 signaling pathway was affected by ARHGAP6 overexpression in breast cancer cells, this study applied active small GTPase pull-

down assays. As a result of ARHGAP6 overexpression, it showed that RhoA activity and ROCK1 protein levels were diminished (Fig. 2F).

Pathway enrichment analysis using the GSEA algorithm revealed that p38 MAPK pathway was significantly enriched in patients with low ARHGAP6 expression (Fig. 2G). In response to ARHGAP6 overexpression, p38 MAPK phosphorylation was dramatically reduced (Fig. 2H).

3.3 ARHGAP6 Silencing Improved Cell Proliferation and Inhibited Ferroptosis in BT-474 Cells Through the RhoA-ROCK1-P38 MAPK Signaling Pathway Activation

To further understand the regulatory role of ARHGAP6 in ferroptosis, BT-474 cells with the highest ARHGAP6 expression compared with other breast cancer were transfected with ARHGAP6 siRNA to knockdown ARHGAP6. BT-474 cells transfected with siARHGAP6 successfully eliminated ARHGAP6 mRNA and proteins (**Supplementary Fig. 1D–F**). Cell proliferation significantly increased, while the level of cell death, Fe^{2+} ion content, and lipid ROS was markedly reduced in the siARHGAP6-transfected cells compared with the siNC-transfected cells (Fig. 3A–D). However, these siARHGAP6-induced changes were reversed by the p38 MAPK inhibitor SB203580 co-treatment (Fig. 3A–D). ARHGAP6 silencing improved p38 MAPK phosphorylation and reduced the suppressive effect of SB203580 treatment (Fig. 3E). Moreover, the expression of GPX4 and SLC7A11 proteins was markedly increased, while the expression of PTGS2, ACSL4, and CHAC1 was markedly decreased in siARHGAP6-transfected BT-474 cells (Fig. 3F). SB203580 exposure further reversed the changes in protein levels of GPX4, SLC7A11, ACSL4, PTGS2, and CHAC1 that were induced by ARHGAP6 silencing (Fig. 3F).

Furthermore, to determine whether RhoA/ROCK signaling mediated the effect of ARHGAP6 on p38 MAPK signaling, siARHGAP6-transfected cells were exposed to RhoA/ROCK inhibitor Y-27632. ARHGAP6 silencing evidently improved RhoA activity and the phosphorylation of p38 MAPK signaling, which were counteracted by exposure to RhoA/ROCK inhibitor Y-27632 (**Supplementary Fig. 2A,B**). This indicates that RhoA-ROCK1-p38 MAPK signaling mediates the effects of ARHGAP6 on ferroptosis in breast cancer.

3.4 ARHGAP6 and RSL3 Induced a Synergistic Effect on Ferroptosis and Tumor Growth in MCF-7 Cells and Mice Models

To evaluate the effects of ARHGAP6 and RSL3 co-treatment on ferroptosis, ARHGAP6-overexpressing MCF-7 cells were stimulated by the ferroptosis-inducer RSL3. This demonstrated that in the MCF-7 cells transduced with pLVX-Puro-ARHGAP6, RSL3 stimulation further decreased cell proliferation (Fig. 4A), enhanced cell death

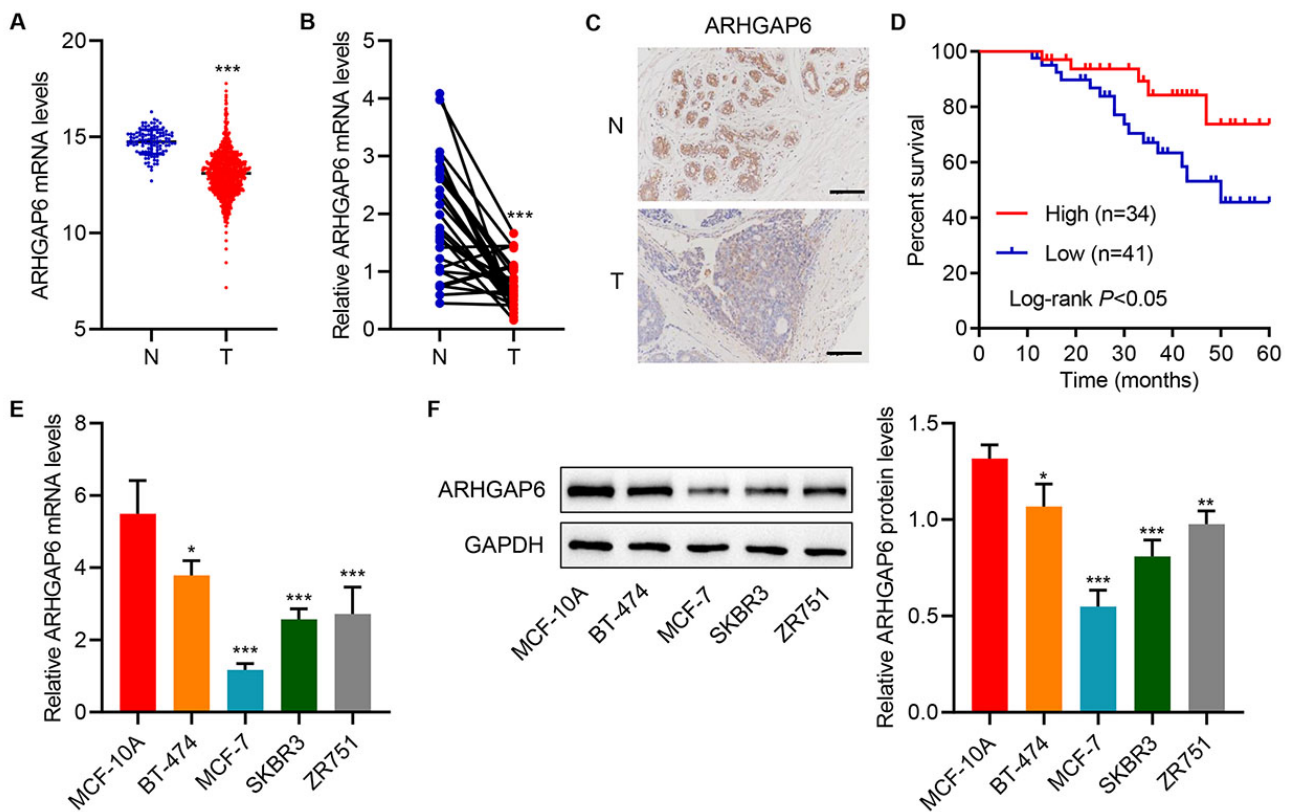


Fig. 1. Rho GTPase-activating protein 6 (ARHGAP6) expression is decreased in tumor tissues and cell lines. (A) ARHGAP6 expression in tumor tissues (T; n = 1104) and adjacent-normal tissues (N; n = 113) in the TCGA database. (B) ARHGAP6 mRNA levels in tumor tissue (T; n = 30) and corresponding adjacent-normal tissue (N; n = 30) in the hospitalized breast cancer patient cohort. (C) ARHGAP6 expression in tumor tissue arrays. (D) Survival of breast cancer patients. (E,F) ARHGAP6 expression in human breast cancer cell lines (BT-474, MCF-7, SKBR3, and ZR751) and nontumorigenic human breast epithelial cell line (MCF-10A) was determined (n = 3). GTPase, guanosine triphosphatase hydrolase enzyme. Scale bar: 100 μ m. * $p < 0.05$, ** $p < 0.01$, *** $p < 0.001$ compared with N or MCF-10A.

(Fig. 4B), Fe^{2+} ion content (Fig. 4C), and lipid ROS accumulation (Fig. 4D), downregulated GPX4 and SLC7A11 expression, and upregulated PTGS2, ACSL4, and CHAC1 expression (Fig. 4E).

To further evaluate the effects of ARHGAP6 overexpression and RSL3 on tumor growth *in vivo*, the mouse-xenograft models were established by subcutaneous injection of MCF-7 cells transduced with ARHGAP6 expression vector and treat with RSL3. Fig. 5A,B shows that the mice with ARHGAP6 overexpression or treated with RSL3 treatment had observably smaller tumor volumes and reduced tumor weights compared to vehicle-treated mice. The combination of two treatments further decreased the tumor volume and weight compared to either treatment alone. Tumor cell proliferation was measured using Ki67 immunofluorescence staining. Either ARHGAP6 overexpression or RSL3 treatment alone significantly suppressed tumor cell proliferation (Fig. 5C,D). Moreover, the combined treatments further suppressed tumor cell proliferation than the induced suppression of each treatment alone (Fig. 5C,D). Protein levels of GPX4, SLC7A11, ACSL4,

PTGS2, and CHAC1 were detected in tumor tissue samples harvested from the mice models. A significant decrease in GPX4 and SLC7A11 protein and a significant increase in PTGS2, ACSL4, and CHAC1 expression were found in mice with ARHGAP6 overexpression or receiving RSL3 injection compared to vehicle mice (Fig. 5E,F). The combined treatments caused more significant changes in these ferroptosis biomarkers compared with each treatment alone (Fig. 5E,F). These observations revealed that ARHGAP6 and RSL3 co-treatment is a better therapeutic strategy for breast cancer than either treatment alone by promoting ferroptosis.

3.5 ARHGAP6 Expression had a Positive Correlation with Ferroptosis Indicators in Breast Cancer

The correlations of GPX4, PTGS2, and CHAC1 with ARHGAP6 in breast cancer tissue and the corresponding adjacent-normal tissue were analyzed. GPX4 as well as SLC7A11 mRNA level was markedly increased, while the mRNA level of PTGS2, ACSL4, and CHAC1 was markedly decreased in cancer tissue com-

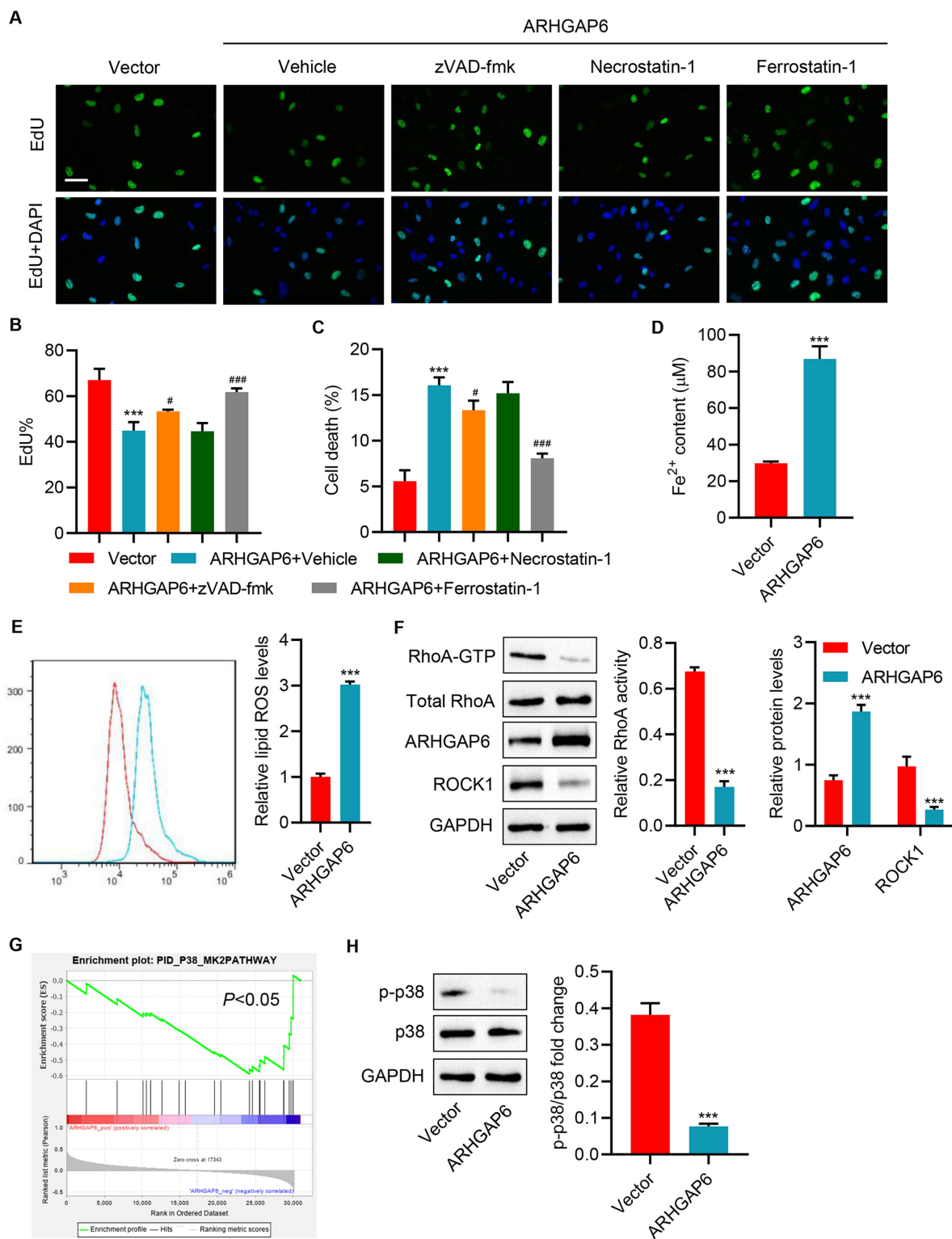


Fig. 2. ARHGAP6 overexpression promotes ferroptosis in MCF-7 cells. MCF-7 cells were infected with indicated lentiviral vectors and treated with 25 μM apoptosis inhibitor zVAD-fmk, 20 μM necroptosis inhibitor necrostatin-1, or 10 μM ferroptosis inhibitor ferrostatin-1, and the (A,B) cell proliferation and (C) cell death were determined ($n = 3$). MCF-7 cells were infected with indicated lentiviral vectors, and the (D) Fe^{2+} ion content, (E) lipid ROS, and the expression of (F) ARHGAP6, ROCK1, RhoA-GTP, total RhoA, and (H) p-p38 and p38 MAPK were determined ($n = 3$). (G) Pathway enrichment analysis using the GSEA algorithm revealed that p38 MAPK pathway was significantly enriched in patients with low ARHGAP6 expression. GSEA, gene set enrichment analysis. Scale bar: 50 μm . *** $p < 0.001$ compared with the blank vector. # $p < 0.05$, ### $p < 0.001$ compared with ARHGAP6 + Vehicle.

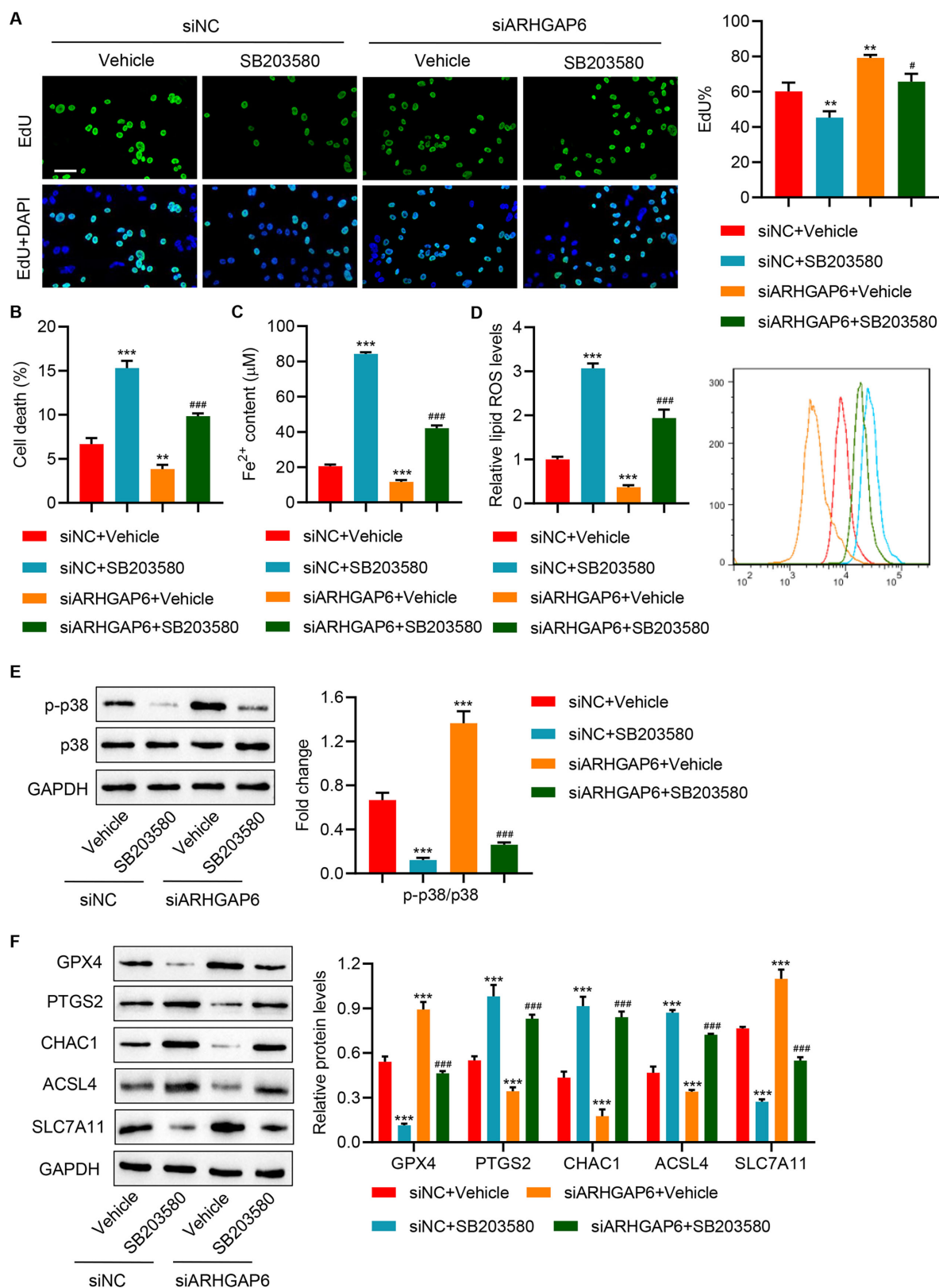


Fig. 3. ARHGAP6 silencing promotes cell proliferation and inhibits ferroptosis of BT-474 cells by activating the p38 MAPK signaling pathway. BT-474 cells were transfected with siARHGAP6 or siNC with or without p38 MAPK inhibitor SB203580 (10 μ M) treatment, and the (A) cell proliferation, (B) cell death, (C) Fe²⁺ ion content, (D) lipid ROS, and expression of (E) p-p38, p38 MAPK, (F) GPX4, PTGS2, CHAC1, ACSL4, and SLC7A11 are determined (n = 3). Scale bar: 50 μ m. ***p* < 0.01, ****p* < 0.001 compared with siNC + Vehicle; #*p* < 0.05, ###*p* < 0.001 compared with siARHGAP6 + Vehicle.

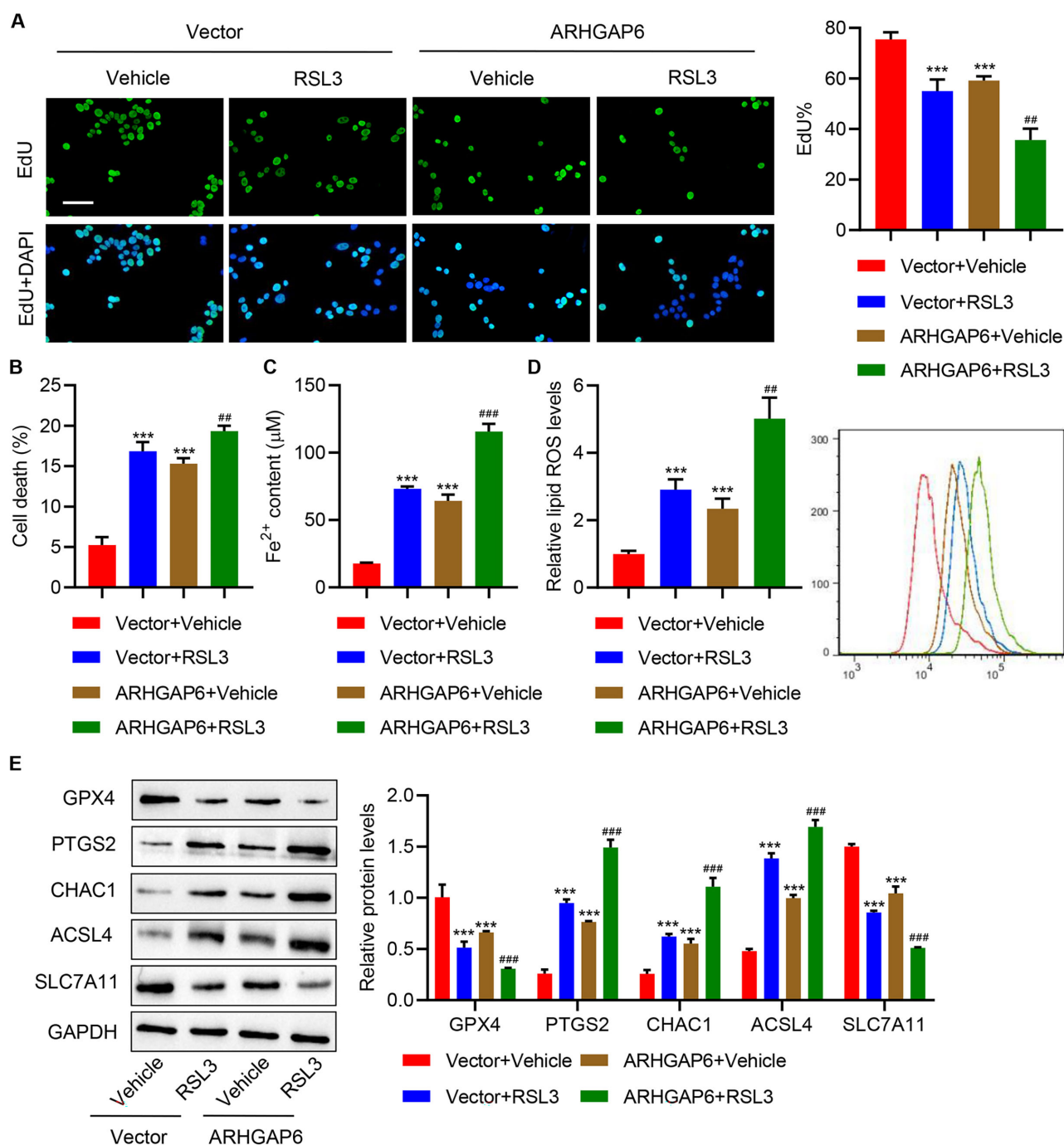


Fig. 4. ARHGAP6 and RSL3 cooperatively inhibit cell proliferation and promote ferroptosis of MCF-7 cells. MCF-7 cells were infected with indicated lentiviral vectors and treated with ferroptosis inducer RSL3 (1 $\mu\text{g}/\text{mL}$), and the (A) cell proliferation, (B) cell death, (C) Fe^{2+} ion content, (D) lipid ROS, and (E) the expression of GPX4, PTGS2, CHAC1, ACSL4, and SLC7A11 were determined ($n = 3$). Scale bar: 50 μm . *** $p < 0.001$ compared with Vector + Vehicle; ## $p < 0.01$, ### $p < 0.001$ compared with ARHGAP6 + Vehicle.

pared with adjacent-normal tissue (Fig. 6A–E). This suggests the inhibition of ferroptosis in breast cancer. GPX4 and SLC7A11 mRNA levels were negatively correlated with the ARHGAP6 mRNA level (Fig. 6F,G). Conversely, PTGS2, ACSL4, and CHAC1 mRNA level was positively correlated with ARHGAP6 mRNA level (Fig. 6H–J). These results demonstrated that ARHGAP6 expression has a sig-

nificant positive correlation with ferroptosis indicators in breast cancer. Additionally, ARHGAP6 is significantly associated with tumor stage ($p = 0.034$), ER status ($p = 0.017$), PR status ($p = 0.020$), and HER2 status ($p = 0.011$; Table 1).

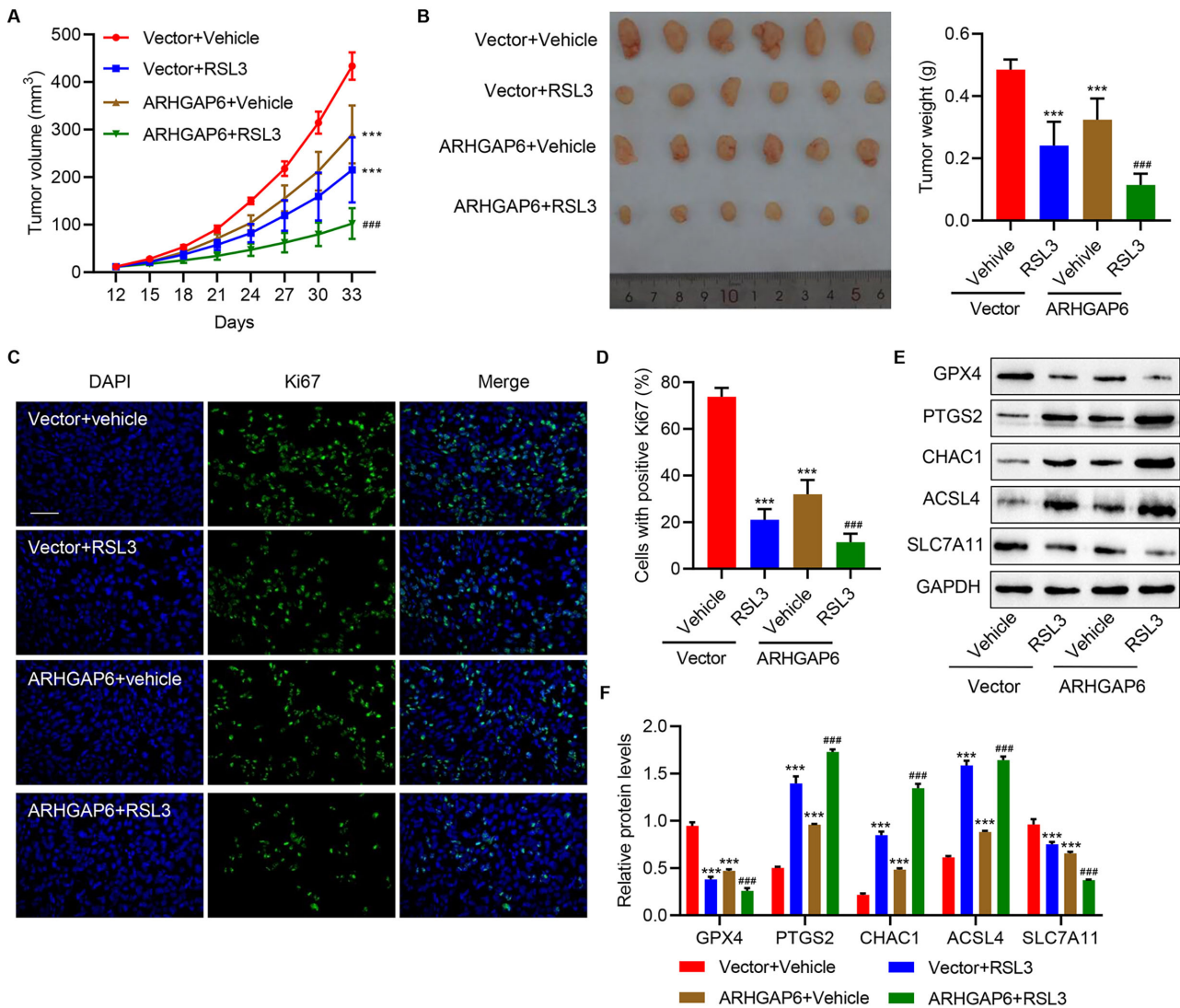


Fig. 5. Cooperative effects of ARHGAP6 and RSL3 on tumor growth *in vivo*. Mice were injected with MCF-7 cells infected with indicated lentiviral vectors, followed by RSL3 (100 mg/kg) injection. The (A) tumor volume (n = 6), (B) tumor weight (n = 6), (C,D) Ki67 immunofluorescence staining (n = 6), and (E,F) the expression of GPX4, PTGS2, CHAC1, ACSL4, and SLC7A11 (n = 3) were measured. Scale bar: 100 μ m. *** p < 0.001 compared with Vector + Vehicle; ### p < 0.001 compared with ARHGAP6 + Vehicle.

4. Discussion

Ferroptosis induction contributes to tumor growth suppression and, therefore, holds great potential for anti-cancer therapy [26]. This study revealed that ARHGAP6 was downregulated in the breast cancer dataset, cancer tissue samples, and cell lines in accordance with previous findings [14,15]. ARHGAP6 overexpression or knock-down strengthened or inhibited ferroptosis, respectively, in breast cancer cells via RhoA-ROCK1-p38 MAPK signaling. Moreover, ARHGAP6 combined with a ferroptosis inducer had cooperative effects on promoting ferroptosis *in vitro* and suppressing tumor growth *in vivo*. This study reports a previously undescribed role of ARHGAP6 in regulating ferroptosis in breast cancer. It expands our understanding on the induction mechanisms of ferroptosis

and has significant implications for developing ferroptosis-mediated therapeutic strategies for breast cancer treatment.

ARHGAP genes turn off Rho-like GTPases that perform multiple functions in the initiation and progression of cancer [14]. It was noteworthy that ARHGAP6 suppresses tumor growth in lung cancer [15,27]. Consistent with these findings, this study showed that in mouse models, ARHGAP6 exhibited a suppressive effect on breast cancer tumor growth, thus proving its role as a tumor suppressor. Ferroptosis is characterized by increased lipid peroxidation and lipid ROS levels and the inactivation of GPX4 responsible for scavenging lipid peroxides [28]. SLC7A11, a subunit unique to system xCT, can synthesize GSH in the intracellular environment and maintain the antioxidant activity of GPX4 [29]. PTGS2 encodes cyclooxygenase 2 (COX-2)

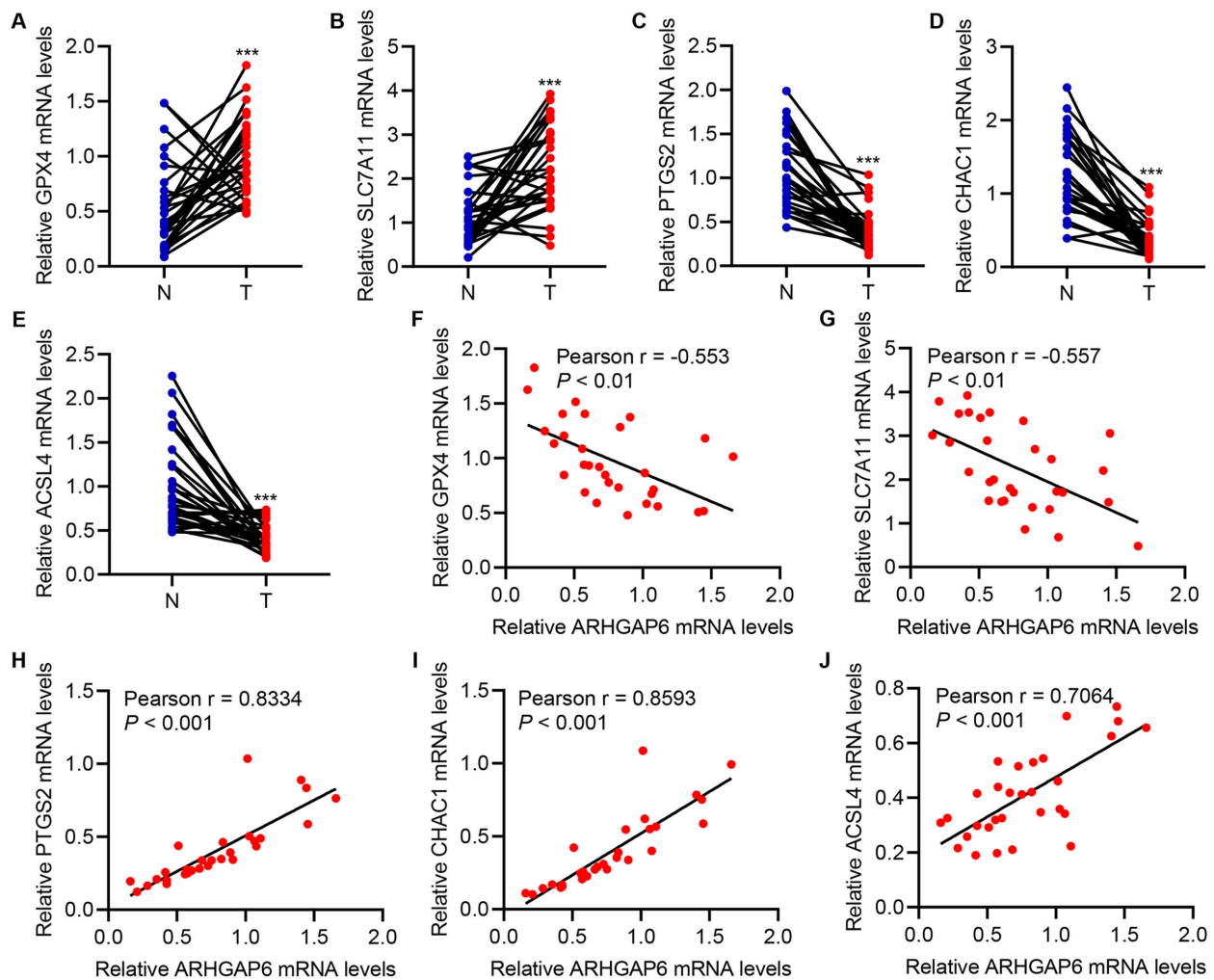


Fig. 6. Correlation analysis in tumor tissues. (A–E) Expression of GPX4, SLC7A11, PTGS2, CHAC1, and ACSL4 in breast cancer tissues (T; $n = 30$) and the corresponding adjacent-normal tissues (N; $n = 30$) in the hospitalized breast cancer patient cohort. (F–J) Pearson correlation scatter plots of tumor tissues ($n = 30$). *** $p < 0.001$ compared with N.

that is upregulated in ferroptosis cells and has been shown to be a downstream target of ferroptosis [30]. Ferroptosis inhibition inactivates the COX-2/prostaglandin E2 pathway [31]. CHAC1 plays an important role in glutathione degradation and is involved in apoptosis, oxidative stress, and ferroptosis [32]. The ACSL4, a crucial lipid metabolism enzyme, contributes to ferroptosis execution [33]. This study found that ARHGAP6 overexpression increased ferroptosis, as indicated by the elevated lipid ROS levels, decreased GPX4 and SLC7A11 proteins, and increased protein levels of PTGS2, ACSL4, and CHAC1. Moreover, the present study provided evidence that ARHGAP6 aggravated RSL3-induced ferroptosis, thereby suppressing tumor growth. Additionally, in tumor tissues, ARHGAP6 mRNA level was negatively correlated with that of GPX4 and SLC7A11 but was positively correlated with that of PTGS2, ACSL4, and CHAC1. This further demonstrates the positive correlation between ARHGAP6 expression and ferroptosis indicators.

RhoA/ROCK signaling pathway is involved in actin-myosin contraction, thereby regulating cellular growth, migration, and differentiation [34]. RhoA/ROCK signaling plays an important role in modulating breast cancer progression by affecting the migration and proliferation of cancer cells [35,36]. A recent study reported that ARHGAP6 influenced the downstream RhoA/ROCK signaling to induce gastric cancer cell death [37]. Similarly, this study found that ARHGAP6 overexpression inhibited RhoA/ROCK1 signaling, indicating that RhoA/ROCK1 signaling mediates ARHGAP6-induced ferroptosis and tumor suppression. p38 MAPK signaling is a key regulator for cancer cell survival and has been widely known as a potential therapeutic target [38]. A significant body of literature provides evidence supporting the regulatory mechanisms of ferroptosis involved in p38 MAPK signaling [19,20]. Consistent with the results of previous studies, this study demonstrated that p38 MAPK signaling mediates ARHGAP6 effect on ferroptosis. Moreover, the difference between p38 MAPK

Table 1. Relationship between ARHGAP6 expression level and clinicopathological parameters of breast cancer.

Variable	ARHGAP6		p value
	High (n = 34)	Low (n = 41)	
Age (years)			0.066
≥58	17	29	
<58	17	12	
Histological type			0.078
Ductal	22	30	
Lobular	8	11	
Other	4	0	
Tumor site			0.069
Left	18	30	
Right	16	11	
American Joint Committee on Cancer (AJCC) stage			0.272
I	5	2	
II	22	26	
III	7	11	
IV	0	2	
Tumor stage			0.034
T1	13	5	
T2	18	25	
T3	2	7	
T4	1	4	
Lymph node status			0.087
Metastasis	14	25	
No metastasis	20	16	
ER status			0.017
Positive	13	27	
Negative	21	14	
PR status			0.020
Positive	10	23	
Negative	24	18	
HER2 status			0.011
Positive	16	31	
Negative	18	10	

activation and RhoA activity induced by ARHGAP6 silencing indicated that other Rho GTPase factors such as Cdc42 or Rac1 may also contribute to the ARHGAP6 silencing-induced p38 MAPK activation [39]. Therefore, further investigation is required to elucidate the role of ARHGAP6-Cdc42/Rac1-regulated p38 MAPK activation in breast cancer.

RhoA/ROCK signaling has been known to activate the downstream p38 MAPK signaling pathway [40,41]. This study showed that RhoA/ROCK signaling inhibition ameliorated the phosphorylation of p38 MAPK induced by ARHGAP6 knockdown in breast cancer cells. Moreover, it revealed that RhoA/ROCK signaling mediates the effect of ARHGAP6 on p38 MAPK signaling, indicating that RhoA-ROCK1-p38 MAPK signaling is an important regulatory mechanism underlying the ARHGAP6 promotion of ferroptosis and suppression of breast cancer tumor growth. Furthermore, evidence revealed that ARHGAP6 upregula-

tion inhibits the downstream STAT3 signaling in regulating the proliferation, migration, and invasion of lung cancer cells [27]. p38 MAPK/NF- κ B/STAT3 signaling, a well-documented inflammatory pathway [42], is speculated as another downstream mechanism of ARHGAP6 involved in ferroptosis in lung cancer.

5. Conclusions

In conclusion, our results showed that by using *in vitro* and *in vivo* experiments, ARHGAP6 inhibits breast cancer tumor growth by strengthening ferroptosis via the targeting of RhoA-ROCK1-p38 MAPK signaling. This study demonstrates the relationship between ARHGAP6 and ferroptosis and advances our knowledge of the regulatory signaling pathways implicated in ferroptosis. ARHGAP6 alone, or in combination with ferroptosis-inducing agents, may be an attractive therapeutic strategy targeting breast cancer.

Availability of Data and Materials

All data presented in this study are included within the paper and its Supplementary files. The data utilized and/or examined in the present study can be obtained from the corresponding author upon a reasonable request.

Author Contributions

XC and DZ designed the research study. XC and JZ performed the research. ZZ, XF, RL, and HL provided help and advice on the acquisition of data and supervision. JZ, XL, and JC analyzed the data. XC and DZ wrote the manuscript. All authors contributed to editorial changes in the manuscript. All authors read and approved the final manuscript. All authors have participated sufficiently in the work to take public responsibility for appropriate portions of the content and agreed to be accountable for all aspects of the work in ensuring that questions related to its accuracy or integrity.

Ethics Approval and Consent to Participate

The medical ethics committee of Southern Medical University Affiliated Maternal & Child Health Hospital of Foshan (No. FSFY-MEC-2021-042) approved the present retrieval method of cancer tissue samples. All patients provided signed informed consent. All animal experiments were performed in accordance with the animal ethics guidelines of the Animal Care and Use Committee of Shanghai Rat@Mouse Biotech Co., Ltd., China [No. 202103(11)].

Acknowledgment

We sincerely thank all who participated in this study.

Funding

This study is supported by Innovation Project of Women and Children medical research center affiliated to Foshan Institute of Fetal Medicine (FEYJZX-2020-006), Foundation of Bureau of Science and Technology of Foshan (2020001005568 and 2220001004898), and Medical Research Project of Foshan Health Commission (20230819A010163).

Conflict of Interest

The authors declare no conflict of interest.

Supplementary Material

Supplementary material associated with this article can be found, in the online version, at <https://doi.org/10.31083/j.fbl2901006>.

References

- [1] Xia C, Dong X, Li H, Cao M, Sun D, He S, *et al.* Cancer statistics in China and United States, 2022: profiles, trends, and determinants. *Chinese Medical Journal*. 2022; 135: 584–590.
- [2] Bray F, Ferlay J, Soerjomataram I, Siegel RL, Torre LA, Jemal A. Global cancer statistics 2018: GLOBOCAN estimates of in-

- cidence and mortality worldwide for 36 cancers in 185 countries. *CA: a Cancer Journal for Clinicians*. 2018; 68: 394–424.
- [3] Yan J, Liu Z, Du S, Li J, Ma L, Li L. Diagnosis and Treatment of Breast Cancer in the Precision Medicine Era. *Methods in Molecular Biology (Clifton, N.J.)*. 2020; 2204: 53–61.
- [4] Wilkinson L, Gathani T. Understanding breast cancer as a global health concern. *The British Journal of Radiology*. 2022; 95: 20211033.
- [5] Mou Y, Wang J, Wu J, He D, Zhang C, Duan C, *et al.* Ferroptosis, a new form of cell death: opportunities and challenges in cancer. *Journal of Hematology & Oncology*. 2019; 12: 34.
- [6] Zeng Y, Cao G, Lin L, Zhang Y, Luo X, Ma X, *et al.* Resveratrol Attenuates Sepsis-Induced Cardiomyopathy in Rats through Anti-Ferroptosis via the Sirt1/Nrf2 Pathway. *Journal of Investigative Surgery*. 2023; 36: 2157521.
- [7] Chen H, Wang L, Liu J, Wan Z, Zhou L, Liao H, *et al.* LncRNA ITGB2-AS1 promotes cisplatin resistance of non-small cell lung cancer by inhibiting ferroptosis via activating the FOSL2/NAMPT axis. *Cancer Biology & Therapy*. 2023; 24: 2223377.
- [8] Guan Z, Chen J, Li X, Dong N. Tanshinone IIA induces ferroptosis in gastric cancer cells through p53-mediated SLC7A11 down-regulation. *Bioscience Reports*. 2020; 40: BSR20201807.
- [9] Chen X, Kang R, Kroemer G, Tang D. Broadening horizons: the role of ferroptosis in cancer. *Nature Reviews. Clinical Oncology*. 2021; 18: 280–296.
- [10] Li Z, Chen L, Chen C, Zhou Y, Hu D, Yang J, *et al.* Targeting ferroptosis in breast cancer. *Biomarker Research*. 2020; 8: 58.
- [11] Wu ZH, Tang Y, Yu H, Li HD. The role of ferroptosis in breast cancer patients: a comprehensive analysis. *Cell Death Discovery*. 2021; 7: 93.
- [12] Mosaddeghzadeh N, Ahmadian MR. The RHO Family GT-Pases: Mechanisms of Regulation and Signaling. *Cells*. 2021; 10: 1831.
- [13] Lawson CD, Ridley AJ. Rho GTPase signaling complexes in cell migration and invasion. *The Journal of Cell Biology*. 2018; 217: 447–457.
- [14] Chen WX, Lou M, Cheng L, Qian Q, Xu LY, Sun L, *et al.* Bioinformatics analysis of potential therapeutic targets among *ARHGAP* genes in breast cancer. *Oncology Letters*. 2019; 18: 6017–6025.
- [15] Li P, Lv H, Xu M, Zang B, Ma Y. ARHGAP6 Promotes Apoptosis and Inhibits Glycolysis in Lung Adenocarcinoma Through STAT3 Signaling Pathway. *Cancer Management and Research*. 2020; 12: 9665–9678.
- [16] Li J, Liu Y, Yin Y. Inhibitory effects of Arhgap6 on cervical carcinoma cells. *Tumour Biology: the Journal of the International Society for Oncodevelopmental Biology and Medicine*. 2016; 37: 1411–1425.
- [17] Chen W, Tan M, Yu C, Liao G, Kong D, Bai J, *et al.* ARHGAP6 inhibits bladder cancer cell viability, migration, and invasion via β -catenin signaling and enhances mitomycin C sensitivity. *Human Cell*. 2023; 36: 786–797.
- [18] Cardone RA, Bellizzi A, Busco G, Weinman EJ, Dell’Aquila ME, Casavola V, *et al.* The NHERF1 PDZ2 domain regulates PKA-RhoA-p38-mediated NHE1 activation and invasion in breast tumor cells. *Molecular Biology of the Cell*. 2007; 18: 1768–1780.
- [19] Hattori K, Ishikawa H, Sakauchi C, Takayanagi S, Naguro I, Ichijo H. Cold stress-induced ferroptosis involves the ASK1-p38 pathway. *EMBO Reports*. 2017; 18: 2067–2078.
- [20] Chang WT, Bow YD, Fu PJ, Li CY, Wu CY, Chang YH, *et al.* A Marine Terpenoid, Heteronemin, Induces Both the Apoptosis and Ferroptosis of Hepatocellular Carcinoma Cells and Involves the ROS and MAPK Pathways. *Oxidative Medicine and Cellular Longevity*. 2021; 2021: 7689045.

- [21] Huang SC, Chen YM, Hu YY, Shi YJ, Xiao QW, Li Z, *et al.* Downregulation of MCF2L Promoted the Ferroptosis of Hepatocellular Carcinoma Cells through PI3K/mTOR Pathway in a RhoA/Rac1 Dependent Manner. *Disease Markers*. 2022; 2022: 6138941.
- [22] Cheng W, Tang Y, Tong X, Zhou Q, Xie J, Wang J, *et al.* USP53 activated by H3K27 acetylation regulates cell viability, apoptosis and metabolism in esophageal carcinoma via the AMPK signaling pathway. *Carcinogenesis*. 2022; 43: 349–359.
- [23] Kuang H, Sun X, Liu Y, Tang M, Wei Y, Shi Y, *et al.* Palmitic acid-induced ferroptosis via CD36 activates ER stress to break calcium-iron balance in colon cancer cells. *The FEBS Journal*. 2023; 290: 3664–3687.
- [24] Zhou Z, Zhao J, Hu K, Hou X, Sun X, Pan X, *et al.* Single High-Dose Radiation Enhances Dendritic Cell Homing and T Cell Priming by Promoting Reactive Oxygen Species-Induced Cytoskeletal Reorganization. *International Journal of Radiation Oncology, Biology, Physics*. 2021; 109: 95–108.
- [25] Li X, Liu J, Chen B, Fan L. A Positive Feedback Loop of Profilin-1 and RhoA/ROCK1 Promotes Endothelial Dysfunction and Oxidative Stress. *Oxidative Medicine and Cellular Longevity*. 2018; 2018: 4169575.
- [26] Lei G, Zhuang L, Gan B. Targeting ferroptosis as a vulnerability in cancer. *Nature Reviews. Cancer*. 2022; 22: 381–396.
- [27] Wu Y, Xu M, He R, Xu K, Ma Y. ARHGAP6 regulates the proliferation, migration and invasion of lung cancer cells. *Oncology Reports*. 2019; 41: 2281–2888.
- [28] Su Y, Zhao B, Zhou L, Zhang Z, Shen Y, Lv H, *et al.* Ferroptosis, a novel pharmacological mechanism of anti-cancer drugs. *Cancer Letters*. 2020; 483: 127–136.
- [29] Do Van B, Gouel F, Jonneaux A, Timmerman K, Gelé P, Pétrault M, *et al.* Ferroptosis, a newly characterized form of cell death in Parkinson's disease that is regulated by PKC. *Neurobiology of Disease*. 2016; 94: 169–178.
- [30] Li Q, Han X, Lan X, Gao Y, Wan J, Durham F, *et al.* Inhibition of neuronal ferroptosis protects hemorrhagic brain. *JCI Insight*. 2017; 2: e90777.
- [31] Xu Y, Liu Y, Li K, Yuan D, Yang S, Zhou L, *et al.* COX-2/PGE2 Pathway Inhibits the Ferroptosis Induced by Cerebral Ischemia Reperfusion. *Molecular Neurobiology*. 2022; 59: 1619–1631.
- [32] Scheffer D, Kulcsár G, Nagyéri G, Kiss-Merki M, Rékási Z, Maloy M, *et al.* Active mixture of serum-circulating small molecules selectively inhibits proliferation and triggers apoptosis in cancer cells via induction of ER stress. *Cellular Signalling*. 2020; 65: 109426.
- [33] Marteau R, Ravez S, Mazhari Dorooee D, Bouchaoui H, Porte K, Devedjian JC, *et al.* Repositioning of FDA-Approved antifungal agents to interrogate Acyl-CoA synthetase long chain family member 4 (ACSL4) in ferroptosis. *Biochemical Pharmacology*. 2022; 204: 115239.
- [34] Haga RB, Ridley AJ. Rho GTPases: Regulation and roles in cancer cell biology. *Small GTPases*. 2016; 7: 207–221.
- [35] Yan L, Li H, An W, Wei W, Zhang X, Wang L. Mex-3 RNA binding MEX3A promotes the proliferation and migration of breast cancer cells via regulating RhoA/ROCK1/LIMK1 signaling pathway. *Bioengineered*. 2021; 12: 5850–5858.
- [36] Zeng Y, Cao Y, Liu L, Zhao J, Zhang T, Xiao L, *et al.* SEPT9_i1 regulates human breast cancer cell motility through cytoskeletal and RhoA/FAK signaling pathway regulation. *Cell Death & Disease*. 2019; 10: 720.
- [37] Komatsu M, Ichikawa H, Chiwaki F, Sakamoto H, Komatsuzaki R, Asaumi M, *et al.* ARHGAP-RhoA signaling provokes homotypic adhesion-triggered cell death of metastasized diffuse-type gastric cancer. *Oncogene*. 2022; 41: 4779–4794.
- [38] Roche O, Fernández-Aroca DM, Arconada-Luque E, García-Flores N, Mellor LF, Ruiz-Hidalgo MJ, *et al.* p38 β and Cancer: The Beginning of the Road. *International Journal of Molecular Sciences*. 2020; 21: 7524.
- [39] Segal L, Etzion S, Elyagon S, Shahar M, Klapper-Goldstein H, Levitas A, *et al.* Dock10 Regulates Cardiac Function under Neurohormonal Stress. *International Journal of Molecular Sciences*. 2022; 23: 9616.
- [40] Zhou H, Sun Y, Zhang L, Kang W, Li N, Li Y. The RhoA/ROCK pathway mediates high glucose-induced cardiomyocyte apoptosis via oxidative stress, JNK, and p38MAPK pathways. *Diabetes/metabolism Research and Reviews*. 2018; 34: e3022.
- [41] Wei YH, Liao SL, Wang SH, Wang CC, Yang CH. Simvastatin and ROCK Inhibitor Y-27632 Inhibit Myofibroblast Differentiation of Graves' Ophthalmopathy-Derived Orbital Fibroblasts via RhoA-Mediated ERK and p38 Signaling Pathways. *Frontiers in Endocrinology*. 2021; 11: 607968.
- [42] Shen Y, Zhang Y, Du J, Jiang B, Shan T, Li H, *et al.* CXCR5 down-regulation alleviates cognitive dysfunction in a mouse model of sepsis-associated encephalopathy: potential role of microglial autophagy and the p38MAPK/NF- κ B/STAT3 signaling pathway. *Journal of Neuroinflammation*. 2021; 18: 246.